Available online at www.sciencedirect.com
SCIENCE DIRECT®
Physics Letters A 346 (2005) 347–354
PHYSICS LETTERS A
www.elsevier.com/locate/pla

Temperature-dependent carrier dynamics in metallic carbon nanotubes

C.W. Chiu [a], Y.H. Chiu [b], F.L. Shyu [c], C.P. Chang [d], D.S. Chuu [b], M.F. Lin [a,*]

[a] *Department of Physics, National Cheng Kung University, Tainan, Taiwan*
[b] *Department of Physics, National Chiao Tung University, Hsinchu, Taiwan*
[c] *Department of Physics, Chinese Military Academy, Kaohsiung, Taiwan*
[d] *Center for General Education, Tainan Woman's College of Art and Technology, Tainan, Taiwan*

Received 7 July 2005; accepted 25 July 2005

Available online 2 August 2005

Communicated by V.M. Agranovich

Abstract

The low energy states in metallic armchair carbon nanotubes can decay by the electron–electron Coulomb interactions with the intraband and the interband excitations. The inelastic scattering rate is very sensitive to the changes in the electronic distribution and the state energy (or the wavevector). The temperature dependence is linear for the Fermi-momentum state. Such dependence is hardly affected by the nanotube radius and the Fermi energy. The electron–electron interactions are more efficient in electronic deexcitations compared with the electron–phonon interactions. The calculated results are roughly consistent with the experimental measurements from the time-resolved photoemission spectroscopy.

PACS: 73.63.Fg; 71.45.Gm

Keywords: Carbon nanotubes; Carrier dynamics

The quasi-one-dimensional (1D) carbon nanotubes were first discovered by Iijima in 1991 [1]. The theoretical study on electronic structures of armchair carbon nanotubes done by Mintmire et al. [2] was earlier than the experimental discovery. Each armchair carbon nanotube owns very special geometric structures and energy bands. There exist armchair and zigzag lines along the azimuthal and axial directions, respectively. Its geometry is characterized by (m, m), where m is the number of dimers along the transverse direction. An armchair (m, m) nanotube is a 1D metal, with the linear valence (π) and conduction (π^*) bands intersecting at the Fermi level ($E_F = 0$). The gapless

* Corresponding author.
E-mail address: mflin@mail.ncku.edu.tw (M.F. Lin).

0375-9601/$ – see front matter
doi:10.1016/j.physleta.2005.07.064

feature remains unchanged even in the presence of the curvature effects (the misorientations of $p\pi$ orbitals and the mixing of $p\pi$ and $sp^2\sigma$ orbitals) [2–7]. The non-armchair carbon nanotubes have narrow or moderate energy gaps. In addition, they can change into metals in the presence of the magnetic flux [7].

Armchair carbon nanotubes should be suitable 1D metallic systems in studying carrier dynamics due to the inelastic electron–electron (e–e) and electron–phonon (e–ph) interactions. The electrical conductivity from the e–ph inelastic scatterings had been calculated from the electron self-energy [8]. At room temperature, the electron lifetime (τ) of the Fermi-momentum state (k_F) is predicted to be 1.4 ps (or the decay rate $1/\tau = 2.85$ meV). In this work, we mainly study the low-frequency electronic excitations, and the deexcitations of the low energy states by means of the inelastic Coulomb scatterings. The dependence of the inelastic scattering rate on the deexcitation mechanisms, the temperature (T), the state energy, the nanotube radius (r), and the Fermi energy (E_F) is discussed. Comparison with the e–ph interactions [8] or the experimental measurements [9] from the time-resolved photoemission spectroscopy is also made.

The unique cylindrical geometry determines band structures and thus electronic excitations. There are a number of theoretical [10–13] and experimental [14–19] studies on the elementary excitations. Due to the cylindrical symmetry, each carbon nanotube exhibits the decoupled electronic excitations of different angular momenta (L's). The low-frequency electronic excitations are only associated with the $L = 0$ mode. This mode is very useful in understanding the many-particle properties of free carriers near the Fermi level. Electrons could be excited from the occupied states to the unoccupied states by the Coulomb or electromagnetic field [9–19]. The excited free carriers further decay by the inelastic e–e and e–ph scatterings. Recently, the experimental measurements of the time-resolved photoemission spectroscopy on metallic single-walled carbon nanotubes have been performed to research the carrier dynamics of the low energy states [9]. The photoexcited electronic distribution returns to the Fermi–Dirac distribution in about 200 fs ($1/\tau \sim 20$ meV) and then relaxes to the initial temperature through the e–ph interactions on a 1 ps scale.

The e–e Coulomb interactions may play an important role on the many-particle properties, the electron lifetime and the electron effective mass. The electron lifetime in metallic and semiconducting carbon nanotubes at $T = 0$ had been studied by means of evaluating the electron self-energy [20]. The previous work shows that the energy dependence of the electron lifetime for various subbands cannot be described by a simple relation. The electron self-energy was also used to investigate the electron effective mass in semiconducting carbon nanotubes [21]. The present study considers the effects of temperature on the electron lifetime in metallic carbon nanotubes. This allows us to compare with the calculated lifetimes with those estimated from the experimental measurements [9] and compare the e–e and e–ph contributions to the deexcitation rates.

We use the tight-binding model and the random-phase approximation (RPA) [10] to calculate the π-electronic structure and the dielectric function (ϵ) of armchair carbon nanotubes. The low-frequency electronic excitations of $L = 0$, which directly reflect the characteristics of the low energy bands, are investigated in detail, e.g., the temperature- and momentum-dependence (q-dependence). They will dominate over the inelastic Coulomb scatterings. The decay rate of the excited free carriers is further evaluated from the *Golden Rule* by Fermi [22]. Our study shows that the inverse lifetime is significantly affected by the electronic distribution (or the decay channels) and the state energy, but not the nanotube radius and the Fermi energy. For the Fermi-momentum state, the inverse lifetime is found to depend on temperature linearly. Moreover, the deexcitation rate is much faster than that caused by the e–ph inelastic scatterings. The calculated results are consistent with the experimental measurements [9].

The π-electronic structure formed by the $2p_z$ orbitals is calculated from the nearest-neighbor tight-binding model. The energy dispersions of the (m, m) armchair nanotube are obtained from diagonalizing the 2×2 Hamiltonian matrix [3]:

$$E^h(k, J) = \pm\gamma_0 \left\{ 1 + 4\cos\left(\frac{\sqrt{3}bk}{2}\right)\cos\left(\frac{\pi J}{m}\right) + 4\cos^2\left(\frac{\sqrt{3}bk}{2}\right)\right\}^{1/2}. \tag{1}$$

The resonance integral for the nearest-neighbor interaction is $\gamma_0 = 3.033$ eV, and $b = 1.42$ Å is the C–C bond length. Electronic states are characterized by the axial wave vector ($|k| \leqslant \pi/\sqrt{3}b$) and the angular momentum

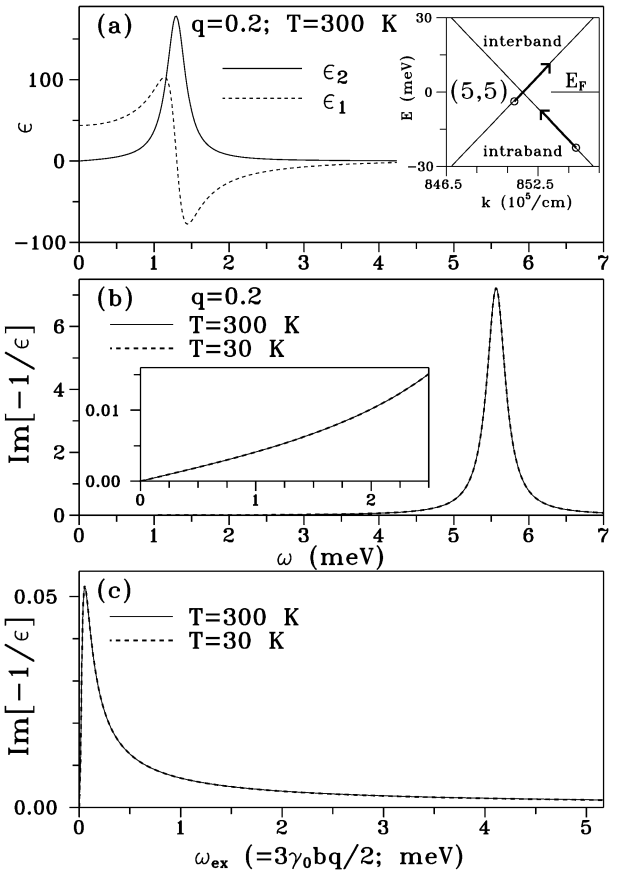

Fig. 1. The $L = 0$ response functions of the $(5, 5)$ nanotube. (a) The real part and the imaginary part of the dielectric function are calculated at $q = 0.2 \times 10^5$ cm^{-1} and $T = 300$ K. The inset shows electronic excitations of the linear energy bands. The loss spectra are evaluated at $T = 300$ K and 30 K for (b) $q = 0.2 \times 10^5$ cm^{-1} and (c) $\omega_{\text{ex}} = 3\gamma_0 bq/2$. The low energy results are also shown in the inset of (b).

$(J = 1, 2, \ldots, 2m)$. $h = c$ and v, respectively, represent conduction and valence bands. The former are symmetric to the latter about the Fermi level $E_F = 0$. The corresponding wave functions are denoted by $\Psi(k, J, h)$. The low-frequency Coulomb excitations are mainly determined by the $J = m$ linear bands closest to the Fermi level (the inset in Fig. 1(a)). Their energy dispersions can be simplified by $E^h(k, J = m) = \pm\frac{3}{2}\gamma_0|k - k_F|$, where $k_F = 2\pi/3\sqrt{3}b$ $(= 851.5 \times 10^5$ cm$^{-1})$. The special linear bands would induce the novel electronic excitations.

For a hollow cylindrical nanotube, the transferred momentum and angular momentum are conserved during the e–e interactions. The low-frequency electronic excitations are characterized by $(q, L = 0)$. The temperature-dependent dielectric function of $L = 0$ within the RPA [10] is given by

$$\begin{aligned}\epsilon(q, L = 0, \omega) &= \epsilon_0 - V(q, L = 0)\chi(q, L = 0, \omega) \\ &= 2.4 - 4\pi e^2 I_0(qr)K_0(qr) \sum_{J,h,h''} \int \frac{dk}{(2\pi)^2} \left|\langle k + q, J, h''|e^{iqy}|k, J, h\rangle\right|^2 \\ &\quad \times \frac{f(E^{h''}(k + q, J)) - f(E^h(k, J))}{E^{h''}(k + q, J) - E^h(k, J) - \omega - i\delta}. \end{aligned} \tag{2}$$

$f(E^h(k,J)) = 1/[1+(E^h(k,J)-\mu)/k_BT]$ is the Fermi–Dirac distribution function. k_B is the Boltzmann constant. The chemical potential μ keeps zero for any T because of the symmetry of the low energy bands about the Fermi level. $\epsilon_0 = 2.4$ is the background dielectric constant contributed from high-energy excitations—other than those excitations within the π-electronic structures. $V(q, L=0) = 4\pi e^2 I_0(qr)K_0(qr)$ is the bare Coulomb interaction of an electron gas. $I_0(qr)$ [$K_0(qr)$] is the first [second] kind of modified Bessel function of zero order. The imaginary part of the response function is associated with the integration of the delta function ($\operatorname{Im}\chi(q, L=0, \omega)$ in Eq. (6)). Under the Coulomb perturbation at $T=0$, there only exist the $v \to c$ interband excitations from the occupied valence states to the unoccupied conduction states. However, at $T \neq 0$, there are, respectively, free holes and electrons in the linear valence and conduction bands. Such carriers cause the intraband excitations from $v \to v$ and $c \to c$. In addition, the RPA had been successfully applied in explaining the many-particle properties of the related 1D quantum-wire systems, e.g., electronic excitations [23,24] and electron distribution function [25,26].

A metallic armchair nanotube exhibits rich excitation properties. The (5, 5) nanotube is chosen for a model study in understanding the essential features of electronic excitations. The imaginary part (ϵ_2) and the real part (ϵ_1) of the dielectric function is shown in Fig. 1(a) at $T = 300$ K and $q = 0.2 \times 10^5$ cm^{-1}. The former, which corresponds to the unscreened single-particle excitations, exhibits a prominent peak at the excitation energy $\omega_{\text{ex}} = \frac{3}{2}\gamma_0 bq$ (equal to the decay energy ω_{de} in Eq. (8)). The latter can change drastically from a positive value to a negative value, as understood from the Kramers–Kronig relations. The zero of ϵ_1 will occur at the plasmon frequency (ω_p), where the loss function, defined as $\operatorname{Im}[-1/\epsilon]$, is very strong (Fig. 1(b)). The single-particle excitations become very weak in the presence of charge screening (the inset in Fig. 1(b)); that is, they are seriously suppressed. The whole excitation spectrum is dominated by the collective excitations (the plasmon). The similar result could also be found in 1D semiconductor quantum wires [23,24].

The plasmon frequency is much higher than the single-particle excitation energy so that the collective excitations absent in the decay channels. The weak single-particle excitations, which own the transferred momentum and energy with the linear relation $\omega_{\text{ex}} = \frac{3}{2}\gamma_0 bq$ (Fig. 1(c)), will take part in the inelastic decay process (Eq. (7)). Furthermore, the small-(q,ω) excitations predominate over the overall electronic deexcitations. It is very special that electronic excitations are almost independent of temperature, as shown in Fig. 1(b) and (c). Both intraband and interband excitations have the same excitation energies, mainly owing to the intersecting linear valence and conduction bands (inset in Fig. 1(a)). Moreover, their bare Coulomb interactions are identical (the product of $V(q, L=0)$ and $|\langle k+q, J, h''|e^{iqy}|k, J, h\rangle|^2$ in Eq. (2)). These two reasons account for the negligible temperature dependence.

We only focus on the deexcitations of free carriers in the linear bands of $J = m$ at any T. They can interact with other electrons by the screened Coulomb interactions of $L = 0$. According to the *Golden Rule* by Fermi [22], the inelastic scattering rate or the inverse electron lifetime of the $(k, J=m, h)$ state is

$$\begin{aligned}\frac{1}{\tau(k,m,h;T)} = 2\pi \sum_{\substack{p,q,J',\\ h',h'',h''',\sigma}} & f\big(E^{h'}(p,J')\big)\big[1-f\big(E^{h'''}(p-q,J')\big)\big] \\ & \times \big[1-f\big(E^{h''}(k+q,J)\big)\big]\big|V^{\text{eff}}\big[(k,m,h,h''),(p,J',h',h'''),(q,L=0)\big]\big|^2 \\ & \times \delta\big(E^{h'''}(p-q,J') + E^{h''}(k+q,m) - E^{h'}(p,J') - E^{h}(k,m)\big), \end{aligned} \tag{3}$$

where the square of the effective e–e Coulomb interaction is

$$\begin{aligned}&\big|V^{\text{eff}}\big[(k,m,h,h''),(p,J',h',h'''),(q,L=0)\big]\big|^2 \\ &\quad = \left|\frac{V(q,L=0)\langle p-q,J',h'''|e^{-iqy}|p,J',h'\rangle\langle k+q,m,h''|e^{iqy}|k,m,h\rangle}{\epsilon[q,L=0,(E^h(k,m)-E^{h''}(k+q,m))]}\right|^2. \end{aligned} \tag{4}$$

By using the two relations

$$\delta\big(E^{h'''}(p-q,J')+E^{h''}(k+q,m)-E^{h'}(p,J')-E^{h}(k,m)\big)$$
$$=\int_{-\infty}^{\infty}d\omega\,\delta\big(E^{h'''}(p-q,J')-E^{h'}(p,J')-\omega\big)\delta\big(\omega+E^{h''}(k+q,m)-E^{h}(k,m)\big) \tag{5}$$

and

$$\frac{\mathrm{Im}[\chi(q,L=0,\omega)]}{\pi[\exp(-\omega/k_BT)-1]}$$
$$=\sum_{p,J',h',h''',\sigma} f\big(E^{h'}(p,J')\big)\big[1-f\big(E^{h'''}(p-q,J')\big)\big]\big|\langle p-q,J',h'''|e^{-iqy}|p,J,h'\rangle\big|^2$$
$$\times\,\delta\big(E^{h'''}(p-q,J')-E^{h'}(p,J')-\omega\big), \tag{6}$$

Eq. (3) is reduced to

$$\frac{1}{\tau(k,m,h;T)}=2\sum_{h'',q}\int_{-\infty}^{\infty}d\omega\frac{-\exp(E^{h''}(k+q,m)/k_BT)}{[\exp(E^{h''}(k+q,m)/k_BT)+1][\exp(-\omega/k_BT)-1]}$$
$$\times\big(-\mathrm{Im}\big[\chi(q,L=0,\omega)\big]\big)\left|\frac{V(q,L=0)}{\epsilon[q,L=0,(E^{h}(k,m)-E^{h''}(k+q,m))]}\right|^2$$
$$\times\big|\langle k+q,J,h''|e^{iqy}|k,J,h\rangle\big|^2\delta\big(\omega+E^{h''}(k+q,m)-E^{h}(k,m)\big). \tag{7}$$

The first term related to the temperature dependence can be further calculated, and the second term is proportional to the loss function. As a result, Eq. (7) is changed into

$$\frac{1}{\tau(k,m,h;T)}=\sum_{h'',q}\frac{\coth(\omega_{\mathrm{de}}/2k_BT)-\tanh((\omega_{\mathrm{de}}-E^{h}(k,m))/2k_BT)}{\exp(-E^{h}(k,m)/k_BT)+1}$$
$$\times\,V(q,L=0)\big|\langle k+q,m,h''|e^{iqy}|k,m,h\rangle\big|^2\,\mathrm{Im}\left[\frac{-1}{\epsilon(q,L=0,\omega_{\mathrm{de}})}\right], \tag{8}$$

where the decay energy $\omega_{\mathrm{de}}=E^{h}(k,m)-E^{h''}(k+q,m)$. There are two kinds of single-particle decay processes, intraband deexcitations ($c\to c$ and $v\to v$) and interband deexcitations ($c\to v$). The temperature-dependent term at $T=0$ becomes $\Theta(E^{c}(k,m)-\mu)\Theta(E^{c}(k,m)-E^{c}(k+q,m))$, i.e., the initial state must be higher than the chemical potential and the finial state. The $T=0$ result is the same with that obtained from the electron self-energy [20]. The contributions due to $\omega_{\mathrm{de}}>0$ are almost the same with those from $\omega_{\mathrm{de}}<0$, because the deexcitations mainly come from the small-(q,ω) electronic excitations. The following discussions will be only focused on the $\omega_{\mathrm{de}}>0$ case.

We first see the inelastic scattering rates of the low energy states at room temperature. The dependence on the wavevector is strong. For the Fermi-momentum state, the interband excitations are the only deexcitation mechanism. $1/\tau(k_F)$ is about 50.9 meV (or $\tau\sim 80$ fs), as shown in Fig. 2(a). When the conduction-band states gradually deviate from the Fermi level, their decay rates grow (the solid curve). There are more vacant states at higher energies according to the Fermi–Dirac distribution function. Such states are responsible for the increase of $1/\tau$ with $|k-k_F|$. The (k,c) states, the k_F state excepted, can be deexcited by the intraband and the interband excitations. The $c\to c$ intraband excitations dominate the decay processes except for these states very close to the Fermi level (the inset in Fig. 2(a)), since they own the small-(q,ω_{de}) transfer, or correspond to the stronger screened response function (Fig. 1(c)). On the other hand, the $v\to v$ intraband excitations are the deexcitation channels of

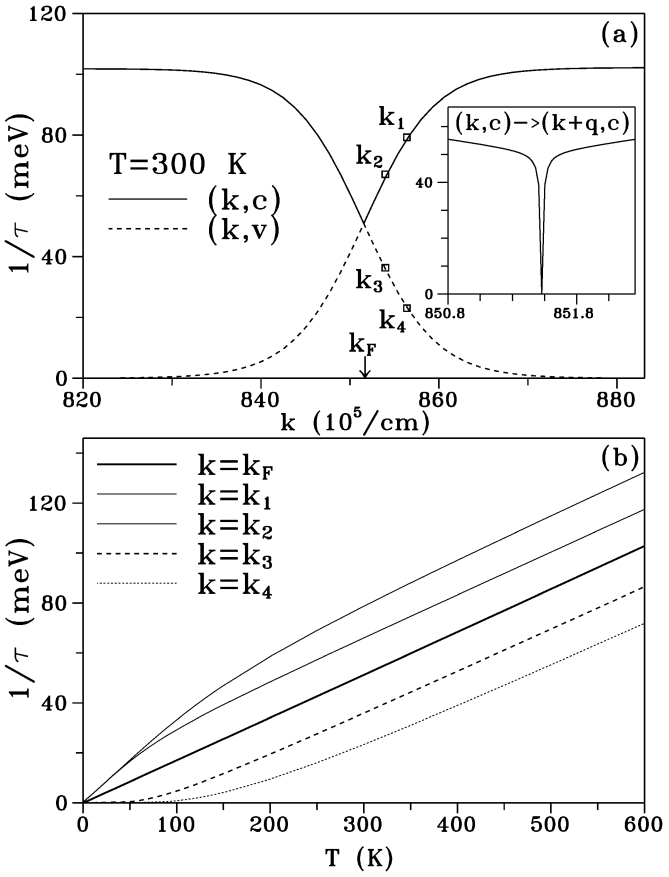

Fig. 2. The inelastic scattering rates of the $(5, 5)$ nanotube. (a) They are calculated for the low energy states at $T = 300$ K. Also shown in the inset are those of the conduction-band states from the intraband excitations. (b) The temperature-dependent scattering rates are shown for different states.

the valence-band states. Their decay rates decline with $|k - k_F|$ quickly (the dashed curve) because of the serious limitation of the electron distribution. $1/\tau$'s are almost vanishing for the (k, v) states with energies lower than $4k_BT$.

The temperature dependence of the e–e inelastic scattering rates is very special. $1/\tau$ of the k_F state depends on temperature linearly, as shown in Fig. 2(b) (the heavy solid curve). The temperature dependence comes from the first term in the right-hand side of Eq. (8). The linear T-dependence is associated with the two conditions, $E^h(k_F, m) = E_F = 0$ and $\omega_{\rm de} \ll k_BT$. Such dependence is identified to be the inverse of $\exp(-\omega/k_BT) - 1$ in Eqs. (6) and (7). When the k_F state interacts with the valence-band states, the available vacant states for the latter are proportional to temperature. Apparently, the electron distributions completely determine the temperature dependence of the inelastic e–e interactions. The similar linear dependence could also be found for the conduction-band states at low temperature ($E^c(k, m) \gg k_BT$), and their scattering rates are enhanced doubly. However, the valence-band states exhibit the nonlinear T-dependence, the composite behavior of T and the exponential decay function ($\exp(E^v(k, m)/k_BT)$). This result relies on the distribution functions of the two interacting electrons.

The inelastic scattering rate of the Fermi-momentum state deserves a closer study. All the armchair carbon nanotubes, as shown in Fig. 3(a), exhibit the similar behavior, the linear T-dependence. The linear bands in metallic carbon nanotubes are the main reason for the special temperature dependence. The decay rate declines slowly as

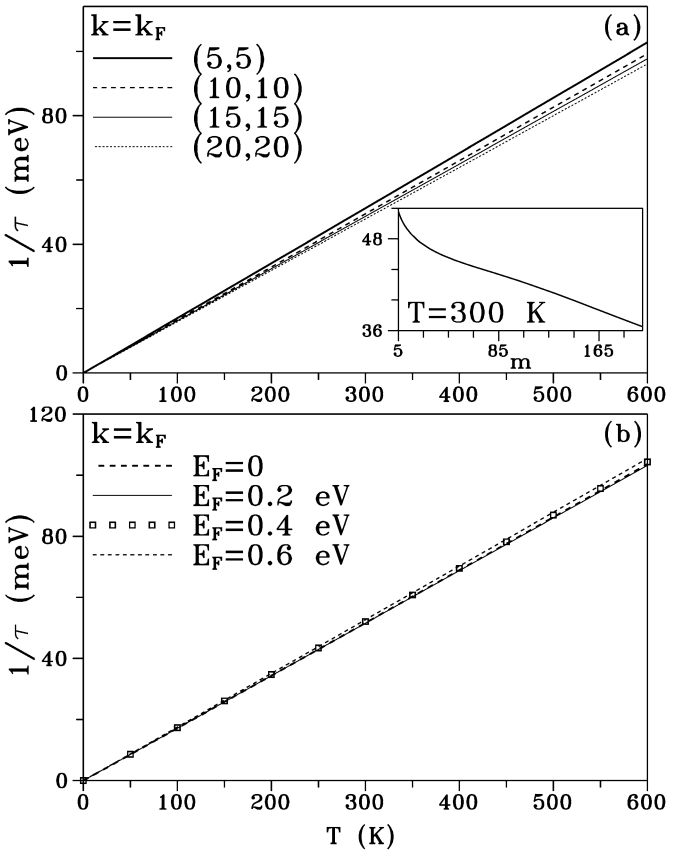

Fig. 3. The temperature-dependent scattering rates of the Fermi-momentum states are calculated for (a) different armchair nanotubes, and (b) the (5, 5) armchair nanotube at various Fermi energies. The inset in (a) shows the radius dependence of the scattering rates at $T = 300$ K.

the nanotube radius grows (inset in Fig. 3(a)). The e–e Coulomb interaction $V(q, L = 0)$ (Eq. (2)) is weaker in a larger nanotube, while the small-q Coulomb interaction depends on the nanotube radius weakly. Hence, that the screened response function in Eq. (8) is predominated by the small-(q, ω) excitations leads to the weak radius dependence.

The Fermi energy could be altered from zero to a finite value, when metallic atoms or molecules are intercalated into carbon nanotubes, as done for graphite. The low-frequency screened response function (Fig. 1(c)) is hardly affected by the Fermi energy ($E_F < 1$ eV), since the electronic excitations almost remain unchanged for the linear energy bands. As a result, the decay rate of the Fermi-momentum state is independent of the Fermi energy. This result further illustrates that the linear energy dispersions determine the electronic excitations and thus the inelastic scattering rate.

From the above-mentioned calculations, the decay rate of the Fermi-momentum state at room temperature is deduced to be $1/\tau \sim 40$ meV for all metallic carbon nanotubes with or without doping. This result roughly agrees with the characteristic deexcitation rate of the metallic carbon nanotubes from the experimental measurements of the time-resolved photoemission spectroscopy [9]. Apparently, the inelastic scattering rate of the e–e interactions is much faster than that ($1/\tau = 2.85$ meV) of the e–ph interactions [8]. The e–e interactions are more efficient in the electron deexcitations. They are expected to play an important role on other physical properties, e.g., the coupling of the e–e and e–ph interactions.

We have calculated for armchair carbon nanotubes the inelastic e–e scattering rates. The special linear energy bands make the e–e interactions exhibit the intraband and the interband excitations. They also result in the temperature-independent loss spectrum. The inelastic scattering rates of the low energy states are dominated by the small-(q, ω) single-particle excitations. The dependence on the electronic distribution and the wave vector is strong. The temperature dependence of the Fermi-momentum state is linear. However, such dependence is hardly affected by the nanotube radius and the Fermi energy. Similar results could also be found in other metallic carbon nanotubes with linear energy bands intersecting at the Fermi level. The inelastic e–e scatterings are more efficient in the electron deexcitations compared with the inelastic e–phonon scatterings. The calculated results could essentially explain the experimental measurements.

Acknowledgements

This work was supported by the National Science Council of Taiwan, under the Grant Nos. NSC 93-2112-M-006-002, NSC 93-2112-M-145-001, and NSC 93-2112-M-165-001.

References

[1] S. Iijima, Nature 354 (1991) 56.
[2] J.W. Mintmire, B.I. Dunlap, C.T. White, Phys. Rev. Lett. 68 (1992) 631.
[3] R. Saito, M. Fujita, G. Dresselhaus, M.S. Dresselhaus, Appl. Phys. Lett. 60 (1992) 2204;
R. Saito, M. Fujita, G. Dresselhaus, M.S. Dresselhaus, Phys. Rev. B 46 (1992) 1804.
[4] N. Hamada, S.I. Sawada, A. Oshiyama, Phys. Rev. Lett. 68 (1992) 1579.
[5] C.L. Kane, E.J. Mele, Phys. Rev. Lett. 78 (1997) 1932.
[6] F.L. Shyu, M.F. Lin, J. Phys. Soc. Jpn. 71 (2002) 1820.
[7] F.L. Shyu, C.P. Chang, R.B. Chen, M.F. Lin, J. Phys. Soc. Jpn. 72 (2003) 454.
[8] R.A. Jishi, M.S. Dresselhaus, G. Dresselhaus, Phys. Rev. B 48 (1993) 11385.
[9] T. Hertel, G. Moos, Phys. Rev. Lett. 84 (2000) 5002.
[10] M.F. Lin, D.S. Chuu, C.S. Huang, Y.K. Lin, K.W.-K. Shung, Phys. Rev. B 53 (1996) 15493.
[11] P.J. Lin-Chung, A.K. Rajagopal, Phys. Rev. B 49 (1994) 8454.
[12] B. Vasvari, Phys. Rev. B 55 (1997) 7993.
[13] M.F. Lin, K.W.-K. Shung, Phys. Rev. B 50 (1994) 17744.
[14] R. Kuzuo, M. Tarauchi, M. Tanaka, Jpn. J. Appl. Phys. 31 (1992) L1484.
[15] T. Pichler, M. Knupfer, M.S. Golden, J. Fink, A. Rinzler, R.E. Smalley, Phys. Rev. Lett. 80 (1998) 4729.
[16] M. Kociak, L. Henrard, O. Stephan, K. Suenaga, C. Colliex, Phys. Rev. B 61 (2000) 13936.
[17] B.W. Reed, M. Sarikaya, Phys. Rev. B 64 (2001) 195404.
[18] H. Kataura, Y. Kumazawa, Y. Minawa, I. Umezu, S. Suzuki, Y. Ohtsuka, Y. Achiba, Synth. Met. 103 (1999) 2555.
[19] M. Ichida, S. Mizuno, Y. Tani, Y. Saito, A. Nakamura, J. Phys. Soc. Jpn. 68 (1999) 3131.
[20] C.W. Chiu, F.L. Shyu, C.P. Chang, D.S. Chuu, M.F. Lin, J. Phys. Soc. Jpn. 73 (2004) 2936.
[21] H. Sakai, H. Suzuura, T. Ando, J. Phys. Soc. Jpn. 72 (2003) 1698.
[22] K.W.-K. Shung, Phys. Rev. B 34 (1986) 1264.
[23] S. Das Sarma, E.H. Hwang, Phys. Rev. B 54 (1996) 1936.
[24] Q.P. Li, S. Das Sarma, R. Joynt, Phys. Rev. B 45 (1992) 13713.
[25] B.Y.-K. Hu, S. Das Sarma, Phys. Rev. Lett. 68 (1992) 1750.
[26] B.Y.-K. Hu, S. Das Sarma, Phys. Rev. B 48 (1993) 5469.